Crystal growth of DAST

ARTICLE *in* CRYSTAL GROWTH & DESIGN · SEPTEMBER 2008

Impact Factor: 4.89 · DOI: 10.1021/cg8003432

3 AUTHORS:

Blanca Ruiz
ETH Zurich
16 PUBLICATIONS **525** CITATIONS
SEE PROFILE

Mojca Jazbinsek
Zurich University of Applied Sciences
188 PUBLICATIONS **1,984** CITATIONS
SEE PROFILE

Peter Gunter
ETH Zurich
483 PUBLICATIONS **8,619** CITATIONS
SEE PROFILE

CRYSTAL GROWTH & DESIGN
2008
VOL. 8, NO. 11
4173–4184

Crystal Growth of DAST

Blanca Ruiz,* Mojca Jazbinsek, and Peter Günter

Nonlinear Optics Laboratory, Swiss Federal Institute of Technology, ETH Zurich, CH-8093 Zurich, Switzerland

Received April 3, 2008; Revised Manuscript Received July 30, 2008

ABSTRACT: We explore the growth of the highly nonlinear optical *trans*-4′-(dimethylamino)-*N*-methyl-4-stilbazolium tosylate) (DAST) crystals from methanol solutions. We determined the key thermodynamic quantities of the DAST/methanol system, which allowed us to optimize the conditions of the crystal growth and to manipulate the size and morphology of the obtained crystals. We developed confined spontaneous nucleation (CSN), a new technique to control the nucleation and produce good quality seeds and platelets for nonlinear optical applications such as the generation of THz waves. We propose the total excess of Gibbs free energy per volume of the solution as a new parameter ($\Delta G/V_{sol}$) that fundamentally affects the growth rate from solution instead of the commonly used supersaturation. This parameter involves also concentration and temperature dependence and is therefore applicable to a large range of growth conditions. A model for the growth dynamics of DAST crystals based on the mass balance equations and the measurements of the growth rate at different experimental conditions allowed us to determine the optimal temperature cooling profile for the growth of large crystals at a constant rate. We also present a numerical analysis of the growth dynamics under various commonly used cooling rates and their effect on the crystalline quality of crystals. It is demonstrated that high quality, record size crystals with dimensions 28 × 28 × 8 mm^3 can be grown with our new optimized cooling profile based on the constant excess of Gibbs free energy density in the solution during the growth.

1. Introduction

Organic materials with very large second-order nonlinear optical (NLO) susceptibilities have attracted a lot of attention because of their potential for high frequency electro-optic modulation,[1−5] frequency conversion[6] and THz wave generation and detection.[7,8] Such materials offer numerous design possibilities and larger and faster optical nonlinearities when compared to their inorganic counterparts.[9,10] Organic crystals are especially interesting because they can offer a highly aligned and stable orientation of NLO chromophores in the crystal lattice. Presently the most well-developed organic NLO crystal is a stilbazolium salt, *trans*-4′-(dimethylamino)-*N*-methyl-4-stilbazolium tosylate) (DAST),[9,11] that exhibits a very large second order NLO susceptibility $\chi^{(2)} = 2020 \pm 220$ pm/V at $\lambda = 1318$ nm and electro-optical figure of merit $n_1^3\, r_{11} = (530 \pm 60)$ pm/V at $\lambda = 1313$ nm.[1] Because of its favorable figures of merit, DAST is a subject of extensive research, starting from the optimization of bulk and thin film growth conditions[4,12−17] to the fabrication of integrated optics elements[2−5,18,19] and generation and detection of THz waves.[7,8,20] High quality crystals of different sizes and orientations have been grown, polished, and, for some applications, coated in our laboratories for the last 15 years. They were used for the determination of the optical, NLO and other physical parameters.[1,6,11,21] In parallel, investigation about fundamental crystal growth for DAST and newly developed next generation nonlinear optical ionic crystals has continued.[22−27]

Much progress has been made in the past few years regarding the growth of DAST crystals. High quality crystals of different sizes and orientations are routinely grown, polished, and mounted in our laboratories for internal research and at our spin off company for commercial purposes.[28] We have built growth cells with high precision temperature control (up to 0.002 °C accuracy) to grow high quality bulk crystals in parallel,[29,30] and a treatment technique for protection from humidity was developed,[31] as well as a new polishing technique that allows us to obtain surface roughness of less than 10 nm.[31,32] DAST also proved to be one of the most efficient materials for THz generation and detection.[8] For this particular application we developed a method for the production of thin ***c***-plates, with which we were able to reduce the growth and preparation time significantly and also to optimize growth for the desired thickness in the ***c*** direction.[33] Considerable efforts have also been done by several groups to control nucleation,[34,35] and to determine the place and position of growth of the nucleated crystals[13,14] as well as to increase the growth rate.[36,37] In this paper we report the fundamental parameters affecting the nucleation and growth of DAST bulk crystals and thin plates. We present a new method to control the nucleation and produce good quality seeds and platelets for THz applications. We analyze and model the dynamics of growth and demonstrate the growth under the optimized growth parameters determined.

Scheme 1. Molecular Diagram of DAST

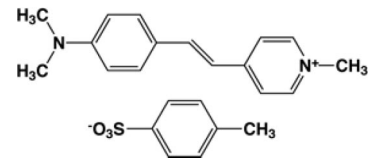

2. Nucleation and Growth Kinetics of DAST

2.1. DAST Basic Characteristics. DAST is a salt composed by a stilbazolium cation, one of the most efficient NLO active chromophores and the tosylate (anion), which induces the noncentrosymmetric macroscopic crystal packing. The chemical structure of DAST is shown in Scheme 1.

DAST crystals belong to the monoclinic space group *Cc* (point group *m*, $Z = 4$) with the lattice parameters $a = 10.365$ Å, $b = 11.322$ Å, $c = 17.893$ Å, and $\beta = 92.24°$. The angles between the dielectric principal axes x_1 and x_3 and the crystallographic axes *a* and *c* are 5.4° and 3.2°, respectively. The x_2 axis is along the *b* axis. The polar axis of the crystal is

* To whom correspondence should be addressed. Fax: +41(0)44 633 1056; tel: +41 (0) 44 633 2927; e-mail: nlo@phys.ethz.ch.

10.1021/cg8003432 CCC: $40.75
Published on Web 09/30/2008

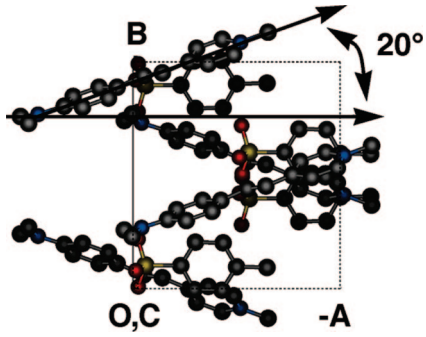

Figure 1. Crystal packing of DAST.

along x_1. A crystal structure analysis showed that the angular deviation of the charge-transfer axis of the stilbazolium chromophores from a completely aligned system is about 20°. Figure 1 shows the packing diagram of DAST crystals.

The melting temperature of DAST is 256 ± 1 °C and its decomposition temperature is 260 ± 5 °C. Hence, the methods based on crystal growth from the melt or evaporation are not suitable for the crystal growth of DAST. Methanol has been found to be the most suitable solvent for the growth of high-quality DAST crystals.

2.2. Thermodynamic Equilibrium of the System DAST/Methanol. The phase diagram of the solute/solvent system is essential for the successful growth of crystals. The main characteristic to resolve is the temperature dependence of the solubility at thermodynamic equilibrium and metastable zone; it not only determines the growth conditions but it also provides useful information for the thermodynamic analysis of the system. In this section we present the phase diagram characteristics of the DAST/methanol system.

The solubility of DAST in methanol as well as its metastable zone has been determined and reported in previous communications.[17] From this data, it is possible to determine the solution enthalpy ΔH and entropy ΔS derived from van't Hoff equation:[38]

$$N = \exp\left(-\frac{\Delta H}{k}\left[\frac{1}{T}\right] + \frac{\Delta S}{k}\right) \tag{1}$$

where N is the molar fraction of DAST in methanol at equilibrium (defined as the amount of moles of solute divided by the total amount of solute plus solvent moles), T is the temperature, and k is the Boltzmann constant. Note that since DAST divides into two ions upon dissolution, the actual entropy and enthalpy changes upon dissolving a molecular entity are $2\Delta S$ and $2\Delta H$, respectively.

In Figure 2 we have plotted the logarithm of the solubility as a function of inverse temperature. From the linear dependence according to eq 1 we can determine, from the slope, the enthalpy change upon dissolution divided by the Boltzmann constant and, from the extrapolation to the infinite temperature, the entropy change ΔS divided by the Boltzmann constant. From our measurements we obtain a solution enthalpy $\Delta H N_A = 43 \pm 2$ kJ/mol and entropy change $\Delta S N_A = 87 \pm 6$ J/°K·mol, where N_A denotes Avogadro's constant.

The solubility of DAST in methanol and the crystallization as a function of temperature are presented in Figure 3 together with the width of the Ostwald-Meyers metastable zone. The measured concentration C (in g of DAST per 100 g of methanol) is related to the molar fraction of DAST in methanol N as $C = (M_{DAST}/M_{meth})N/(1 - N)$, where M_{DAST} and M_{meth} are the molar weights of DAST and methanol, respectively. The curves are

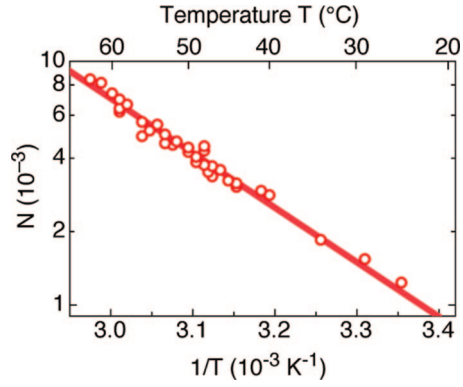

Figure 2. Measured molar fraction (in logarithmic scale) of DAST in methanol at the saturation temperature as a function of the inverse temperature. The solid line is according to eq 1.

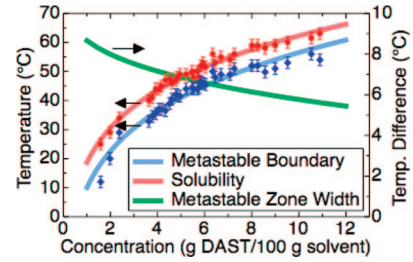

Figure 3. Saturation temperature (red curve), homogeneous nucleation temperature (blue curve), and metastable zone width (green curve) of DAST in methanol as a function of concentration. The scale on the right corresponds to the metastable zone width.

according to eq 1 considering the data of Manetta et al.[17] The width of the metastable zone, which is the difference between the equilibrium temperature and the temperature at which spontaneous nucleation occurs, slightly diminishes with increased concentration.

2.3. Nucleation Theory. From nucleation theory it follows that the change in the Gibbs free energy associated with one solute nucleus ΔG_n will contain contributions mainly from the difference in volume energy between the crystal and the solution (binding energy) and from the interfacial surface energy.[38,39] The change in the Gibbs free energy for a single nucleus can be therefore written as

$$\Delta G_n = n4\pi r^2\gamma - \frac{4}{3}\pi r^3\frac{\Delta G}{v} \tag{2}$$

where the cluster considered is a sphere with radius r, γ is the interfacial energy, ΔG is the change of Gibbs free energy per crystallized molecule, and v is the specific volume of the solute molecule (in our case we consider the volume of the two ions together).

Consider a solution at temperature T with a concentration C that is above the equilibrium concentration $C_{eq}(T)$. The difference of the Gibbs free energy ΔG per molecule between the solid and the liquid is

$$\Delta G = kT\ln(S) = kT\ln(1+\sigma) \tag{3}$$

where T is the temperature at which the transformation occurs, $S = C/C_{eq}$ the saturation ratio, and σ is the relative supersaturation defined as

$$\sigma = \frac{\Delta C}{C_{eq}(T)} = \frac{C - C_{eq}(T)}{C_{eq}(T)} \tag{4}$$

and considering eq 1, we can write the saturation ratio as

$$S = \exp\left(\frac{\Delta H \Delta T}{kTT_{eq}(C)}\right) \quad (5)$$

with ΔT defined as $\Delta T = T_{eq}(C) - T$ where $T_{eq}(C)$ is the temperature at equilibrium and T is the actual temperature at a certain solution concentration C. Therefore, the excess free energy of a supersaturated solution may be written as

$$\Delta G = kT \ln S = \frac{\Delta H \Delta T}{T_{eq}(C)} \quad (6)$$

From eq 2 it is easy to see that the Gibbs free energy of a nucleus will first increase as the nucleus grows because of the surface energy created, until it reaches a maximum at a critical point called the critical radius r^*, after which it will decrease with every extra molecule that attaches to it, which makes the nucleus stable. The critical radius is then

$$r^* = \frac{2\gamma v}{\Delta G} \quad (7)$$

and the value of ΔG_n for a single nucleus of critical size is

$$\Delta G_n^* = \Delta G_n(r^*) = \frac{16\pi\gamma^3 v^2}{3\Delta G^2} \quad (8)$$

By considering that the critical nucleus is composed of i^* molecules $i^* = 4/3\pi r^{*3}/v$, we can determine the number of molecules in the critical nucleus for a certain excess of free energy ΔG, if we can determine the surface energy γ. We can also estimate this number by using the following expression derived for cubic crystals.[39]

$$i^* = \left(\frac{2\Delta H}{3\Delta G}\right)^3 \quad (9)$$

The frequency of formation of a particle with a radius r^* is called the nucleation rate and is proportional to the probability of the formation of a nucleus $\exp(-\Delta G_n^*/kT)$

$$J = J_0 \exp\left(-\frac{\Delta G_n^*}{kT}\right) \quad (10)$$

The induction period τ_i is inversely proportional to the frequency of formation of nuclei $\tau_i \propto J^{-1}$ and its value can be determined experimentally and it is related to the surface energy γ by means of

$$\tau_i = \tau_{i0} \exp\left(\frac{16\pi\gamma^3 v^2}{3k^3T^3(\ln S)^2}\right) \quad (11)$$

2.4. Mass Balance during the Growth. In this subsection we consider the mass of solute used by the crystal for its growth and the balance with the solute left in the solution, in order to evaluate the concentration of the solution as a function of time during growth. We consider the growth rate for a surface of the crystal as

$$f = \frac{dx}{dt} = f(\sigma, C, T) \quad (12)$$

where $x(t)$ is the length of the crystal perpendicular to the surface. The growth rate is in many cases given only as a function of the relative supersaturation σ at the liquid−crystal interface. We however also consider here that the growth rate tends to be larger for higher concentrations and higher temperatures for the same amount of supersaturation. Growth rates for organic crystals grown from solution are usually reported to be in the order of 1 mm/day for well-stirred systems.[40]

The additional mass of material grown at a single surface of the crystal during the time t can be written as

$$m_A(t) = \int_0^t A(t') \cdot f(t') \cdot \rho \cdot dt' \quad (13)$$

where ρ is the mass density of the crystal. The total amount η_{crys} of material crystallized (in moles) is simply the sum of material attached to all growth faces of the crystal, divided by the molar weight of DAST, M_{DAST}

$$\eta_{crys}(t) = \frac{m_A(t) + m_B(t) + m_C(t) + ...}{M_{DAST}} \quad (14)$$

We now consider a growth cell with a total volume of solution V_{sol} with a molar fraction of solute N. The total amount of solute in moles η_{DAST} present in the system before seeding is then

$$\eta_{DAST} = \frac{N \cdot \rho_{meth} \cdot V_{sol}}{(1-N)M_{meth}} \quad (15)$$

where ρ_{meth} is the density of the solvent and M_{meth} is the molar weight of the solvent.

During growth (i.e., after seeding) the amount of solute available in the solution is the difference between the total amount η_{DAST} and η_{crys}, so at any given time t the new equilibrium temperature can be calculated from eq 1 as

$$T_{eq}(t) = \frac{\Delta H}{\Delta S - k \ln(N(t))} \quad (16)$$

with $N(t)$ the new molar fraction of solute in the solution

$$N(t) = \frac{\eta_{DAST} - \eta_{crys}(t)}{(\eta_{DAST} - \eta_{crys}(t)) + \eta_{meth}} \quad (17)$$

The change of solution concentration because of the amount of the material grown is then considered to evaluate the supersaturation during the growth. We should also take care that supersaturation does not exceed the limits of the Ostwald-Miers diagram (i.e., Figure 3) as we wish to avoid homogeneous nucleation.

2.5. Driving Force for the Crystallization and Cooling Rate. For the growth of crystals from solution, a linear cooling rate is most often chosen since it is the most convenient in terms of technological implementation. However, there is no physical reason for such a cooling rate and it does not represent ideal conditions for the constant growth of bulk crystals. A cubic decay in the temperature has been proposed by several authors[39] by considering the volume change of the seed. However, for low temperature solution growth like the one we deal with in this paper, the change in solubility with temperature is far from linear. Instead we choose a cooling rate that provides a constant excess free energy per unit volume of solution that in turn provides a constant equilibrium between the free energy of the solution and the attachment energy of a monolayer of the crystal growing from it, as explained in the following paragraph.

If one considers a given amount of solution surrounding the crystal with a certain excess Gibbs free energy ΔG per molecule given by eq 3, which results from cooling the solution to a temperature T below the equilibrium temperature T_{eq}, we have a total amount of free energy difference

$$\Delta \mathbf{G} = \Delta G \cdot N_A(\eta_{DAST} - \eta_{cryst}) \quad (18)$$

between the solution and the grown crystal, which will again be zero once the crystal grows large enough to restore equilibrium at T. We can regard ΔG as the driving force for crystallization.

If we consider the dependence of the growth rate on ΔG to have a simple form $f = a\Delta G$, where a is a constant, it is clear that the growth rate will decay as we approach the equilibrium; hence, for keeping the growth rate constant we should also maintain a free energy difference with the solution from which it is growing.

There is also the restriction that a crystal can only interact with a given amount of solution in any period of time. This amount of solution will be determined by the diffusion constant, which is a property of the materials involved. This means we need to consider the quantity of free energy per unit volume of solution surrounding the growing crystal,

$$\Delta G_{\mathrm{Vsol}} = \frac{\Delta G}{V_{\mathrm{sol}}} \tag{19}$$

In order to maintain a constant growth rate this quantity should be kept constant.

2.6. Growth Rate. As mentioned above, there is an effective amount of solution with which a growing crystal can interact at any given moment; this is determined by the diffusion constant D and the concentration gradient. The net flux of solute molecules that reaches the growing face of the crystal is determined by Fick's law of diffusion and it is a function of the excess of molecules per unit solution. Although in our case the solute is composed of two ions that may diffuse at different rates, we assume the diffusion constant to be an average of the two. Moreover, the ionic nature from the solute molecules contributes to a homogeneous mix of the two components in the solution and we can presume that as long as no field is applied to the solution, there is no reason for a significant separation of the components. A comprehensive explanation of the growth from solutions and a derivation of the growth rate dependence on the growth parameters has been given by Bennema.[41] We have chosen a simplified version of the growth rate to describe our results, in which the growth rate f is a function of ΔG_{Vsol} and has the following form

$$f = B_1 \cdot (\Delta G_{\mathrm{Vsol}})^2 \tanh\left(\frac{B_2}{(\Delta G_{\mathrm{Vsol}}{}^2}\right) \tag{20}$$

where B_1 and B_2 are constants of the system.

We aim to achieve a constant growth rate of our crystals to ensure homogeneity. In our evaluation of the optimal temperature profile for the controlled growth we keep a constant ΔG_{Vsol} throughout the whole experiment.

In Section 4.3.c we will present the calculations of the optimum cooling rate and the experimental conditions that allow us to achieve such growth rates.

3. Growth Kinetics of DAST

3.1. Crystal Morphology and Growth Mechanisms. The growth habit of a crystal when grown from methanol is presented in Figure 4. When grown from methanol, DAST crystals grow naturally as ***ab*** platelets.

While the preferential growth direction for DAST crystals is along the ***a***-axis, the actual attachment of new cells and growth on the ***a***-direction occurs only when the (111) and (1$\bar{1}$1) faces are present, as well as (11$\bar{1}$) and (1$\bar{1}\bar{1}$). If these faces are removed from the morphology of the crystal the attachment barrier becomes too large for successful growth. In this case the crystal can only start new layers on the edges of (001) and (00$\bar{1}$) faces with each layer growing in the -***a*** direction until it is finished. Such a growth is characterized by a thickening of the crystal while maintaining an almost constant ***ab*** area.

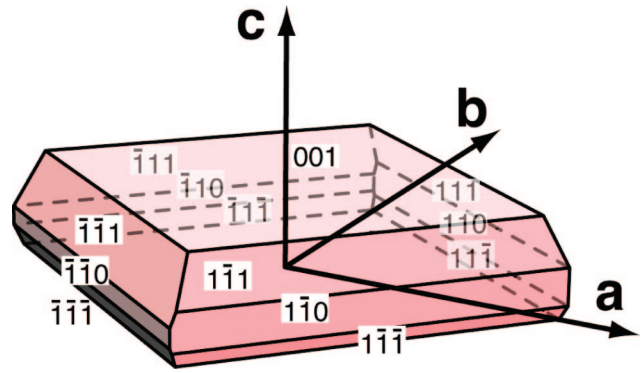

Figure 4. Growth habit of DAST crystals grown from methanol. The fastest growth direction is along the crystallographic ***a*** or [100] direction.

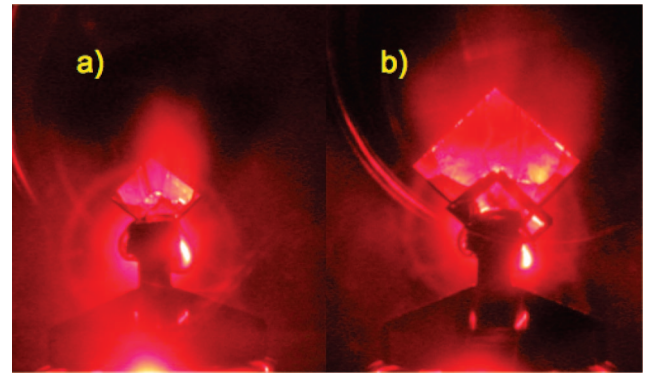

Figure 5. Crystal growing without (11$\bar{1}$) and (1$\bar{1}\bar{1}$) faces. The photographs were taken (a) on the 24th day of growth and (b) on the 44th day of growth. The twin is slightly visible already on the earlier stage of the growth and it is much better developed in the (b) section of the photograph.

Furthermore, it has been observed by several authors[33,42,43] that at higher concentrations the crystals obtained tend to be thicker (smaller ***a/c*** ratio) than those grown at lower concentrations.

The area of the (111) and (1$\bar{1}$1) faces tends to be larger than that of (11$\bar{1}$) and (1$\bar{1}\bar{1}$) and thus slightly more stable and prone to stay visible in the final morphology of the crystal. If however, by special circumstances of the growth, the later two faces shall disappear, the crystal develops a "curved" (00$\bar{1}$) surface as a consequence. The growth of the crystal after this gets slower at best and fully halted and defective in most cases. In any case it makes the cutting and orientation of the crystal after the growth much more complicated as large volumes must be polished away to obtain flat faces and a large portion of the crystal is wasted.

It should be noted that the calculations done for the growth in our optimized cooling rate experiments (see later) assume that the growth rate of the seed is constant and not interrupted or obstructed in any way. For the case when faces (11$\bar{1}$) and (1$\bar{1}\bar{1}$) disappear from the morphology, the edge of the crystal becomes sharp and the attachment of the new cells slows down. In this case the cooling rate calculated for a normally shaped crystal does not work well. Crystals with a curved (00$\bar{1}$) face usually create a twin on this face that allows it to continue growth at an almost regular rate. The twin has usually a 180° rotation around the ***a***-axis so that on both sides of the final crystal there is a (001) face.

Figure 5 shows a photograph of a crystal which has lost its (11$\bar{1}$) and (1$\bar{1}\bar{1}$) faces and become curved on the (00$\bar{1}$) side.

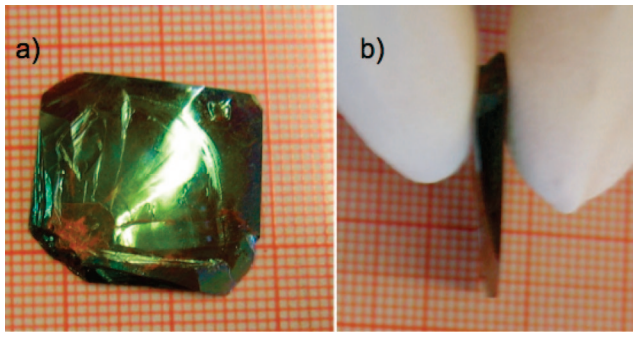

Figure 6. Crystal grown without $(11\bar{1})$ and $(1\bar{1}\bar{1})$ faces. Panel (a) shows the crystal from the $(00\bar{1})$ perspective. The curved face makes cutting and polishing a complicated task. (b) The side view of the same crystal; the lower portion of the photograph shows the sharp ending at the ***a***-tip.

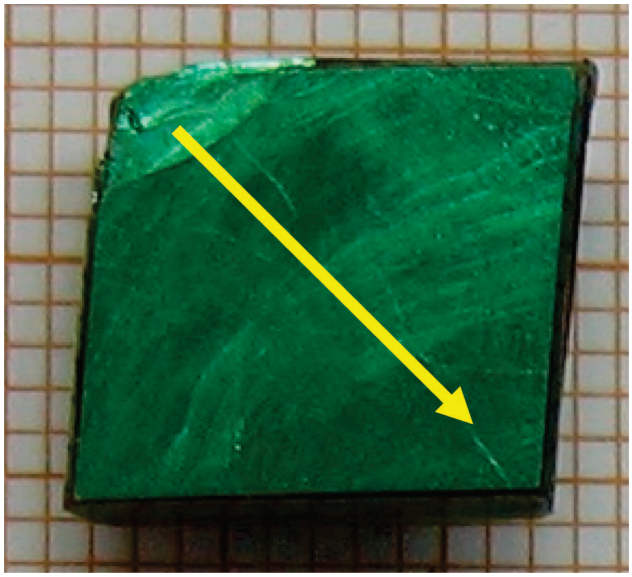

Figure 7. As grown crystal showing growth steps on the (001) face. The arrow indicates the crystal growth direction ***a***.

Figure 6 shows the final result of a growth with missing morphological faces. Although the crystal quality is optically good, such crystals are only of limited use because of the complexity of the postprocessing: the crystal must be first cut and planarized by polishing, which is not only time-consuming but it also increases the risk of damaging the crystal.

Figure 7 shows a photograph of the (001) surface of an as-grown crystal with $(11\bar{1})$ and $(1\bar{1}\bar{1})$ faces present, in which it is possible to observe the steps originating on the tip of the crystal and growing toward the -***a*** direction.

The cell that attaches on a flat surface free-standing or on an incomplete edge has a higher probability of being detached again when compared with those in a complete edge or inside of a surface, because the latter have more nearest neighbors. The positions making up a (111) plane and kinks on [100] steps are called half-crystal positions because they offer an attachment energy of exactly half of that experienced by a molecule situated inside of the crystal (for an anisotropic material it can happen that it is not exactly half but still close enough to make it plausible). These positions also happen to have the mean attachment energy of the crystal.

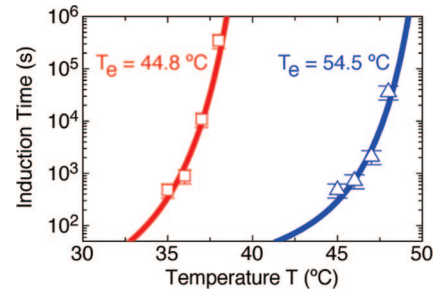

Figure 8. Induction time τ_i (see text) as a function of temperature for DAST/methanol solutions together with the theoretical curves according to eq 11. The red squares represent the data obtained for a concentration with an equilibrium temperature $T_e = 44.8$ °C and the green triangles are for a solution with $T_e = 54.5$ °C.

4. Experiments and Numerical Calculation

4.1. Nucleation. The control of nucleation of DAST crystals is of great importance for the generation of seeds used for bulk growth. Additionally, it presents an important step for the direct growth of thin plates for THz applications, without a need for additional cutting/resizing, which requires very specific growth conditions for a given final desired size. We have therefore first investigated the nucleation conditions for DAST crystals.

With the help of the nucleation theory presented in Section 2.3 and the experimental data for the metastable zone, we have estimated the critical nucleus size and established its dependence on the concentration of the solution.

By using eq 9 that is a very simplified expression for cubic crystals, we estimated the critical amount of molecules in a critical nucleus as a function of the equilibrium temperature T_{eq}. The size of the critical nucleus corresponds to a range from 30 to 45 molecules per side for a cubic formation or a radius of 14 to 22 nm for a sphere.

By using the latent heat data obtained from the solubility measurements presented on Section 2.2, the expression (7) for the critical radius and the simplified expression (9) for the critical amount of molecules i^*, we can estimate the order of magnitude of the interfacial tension, which gives $\gamma \approx 20$ mJoule/m^2.

Another way to obtain the interfacial tension is by measuring the induction time τ_i, which is the time needed for the formation of critical nuclei at a certain temperature and concentration, as described by eq 11. We have measured the induction time for different concentrations. The induction time was measured by heating known amounts of DAST and methanol up to 10 °C above the equilibrium temperature while stirring. The temperature was kept high for an hour after all visible particles had disappeared to ensure total dissolution of precursor embryos. After this time, the temperature was lowered to a chosen setpoint below equilibrium and the time was measured from the moment it reached the setpoint temperature until the first nucleus appeared. The time between the appearance of a critical nucleus and its growth to a visible size is small enough to be neglected. The solution was then allowed to redissolve in the same manner as described above and a new supersaturation point was chosen for measurements. This procedure was repeated for various supersaturations for each of the concentrations measured.

Using the theoretical relation (11) to describe the temperature dependence of the induction times obtained experimentally at certain concentrations (see Figure 8) allowed us to estimate the interfacial tension γ to be 3.0 ± 0.3 mJ/m^2 for the solution with a concentration of 4.27 g of DAST per 100 g of methanol, which corresponds to an equilibrium temperature of 44.8 °C; for the solution with concentration 6.94 g of DAST per 100 g

of methanol corresponding to an equilibrium temperature of 54.5 °C we estimated γ to be 2.6 ± 0.3 mJ/m^2.

The values for the superficial tension obtained with the above data are about 5−10 times lower compared to the value obtained by the estimation (9) using the latent heat of the solution.

Other authors have recently measured the induction time for a DAST/methanol solution and obtained interfacial tension values that range from 2.4−3.8 mJ/m^2, which is in good agreement with our results.[15,16] Organic crystals are chemically bonded by van der Waals forces, hydrogen bonds and Coulomb forces, which are weaker than the covalent bonds that exist between atoms of metallic crystals. These bonds between molecules are primarily responsible for the bulk properties of the matter, such as surface tension. It is for this reason that while it is common to find surface tensions of a couple hundreds of mJ/m^2 in metallic crystal−liquid interfaces this value tends to be on the order of tens of mJ/m^2 for organic crystals.

We have carried out the measurements of the induction time with and without the presence of a growing crystal to observe its effect on secondary nucleation. The time measured in both cases was practically identical. An important result obtained from these measurements is the effective growth time for supersaturated solutions before secondary nucleation occurs.

For the case when the final goal is to grow a large crystal, the induction time is the limiting factor to be considered. There is a trade off between the growth rate and the total time one crystal growth run can last, which should be considered in the design of the growth experiment.

4.2. Controlled Nucleation (Seeds). We have investigated different methods to control nucleation to produce seeds of high quality for the growth of large crystals. In addition, small single crystalline plates are needed for the generation and detection of THz waves. There are various possibilities to produce nucleation in a more or less controlled manner in a growth cell: local cooling, impurity introduction, laser induced nucleation, and confined spontaneous nucleation to name a few. Although most authors favor spontaneous nucleation for the generation of seeds,[12−14] this normally occurs in regimes where growth conditions are not favorable for the production of high quality crystals. The position of the crystals after the nucleation occurs has been already identified by several groups as crucial for the unimpeded growth of the crystallites after their creation.[13,14] Mori et al. developed the slope nucleation method (SNM), which is a simple and effective way to promote the vertical position of the crystals. A ridged bottom of the vessel is also useful for this purpose. To overcome the tradeoff between the nucleation rate and the crystal quality at the high supersaturations necessary for spontaneous nucleation, the induced nucleation was achieved by Tsunesada et al. by illumination of the growth vessels with a pulsed laser. Laser induced nucleation is an elegant solution,[14,44] although in most cases unnecessary.

4.2.a. Confined Spontaneous Nucleation (CSN). The most important factors for the successful growth of seeds or small plates is to keep the number of seeds small and to provide favorable conditions of moderate supersaturation and temperature of the solution for the subsequent growth of the generated nucleus. In this subsection we describe a new technique we developed for the controlled generation of high quality seeds, which allows us to optimize both the amount of seeds and their growing environment.

A simple way to provoke nucleation inside of the metastable zone is to introduce a cold needle in the solution to provide a local point of nucleation; also introducing a few particles of solute powder effectively supplies a nucleation point as these

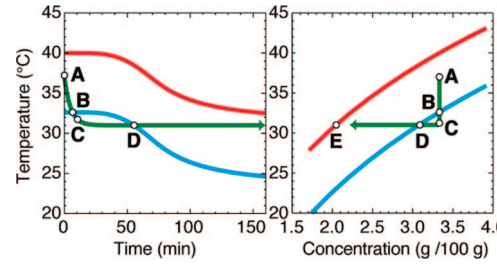

Figure 9. Temperature of the solution (green) and the metastable zone boundaries (red and blue) as functions of time and concentration during CSN; a schematic drawing. A: start of the experiment. B: the temperature of the solution reaches the edge of the metastable zone. C: the induction time is reached; nucleation and start of the growth. D: the concentration of the solution decreases due to the growth and falls within the metastable zone again, from D on the nuclei grow until the equilibrium concentration is reached (point E).

can no longer be dissolved when the solution is below the equilibrium temperature. Nevertheless, we prefer a more controllable way to know the approximate number of produced nuclei. It is for this reason that we favor the confined spontaneous nucleation (CSN). In this method the mother solution is prepared and heated above the equilibrium temperature where it is kept for a few hours to ensure the dissolution of all precursor embryos. The bottles are closed with a cap that has an integrated pipet on the top, which is not in direct contact with the solution to avoid nucleation centers. After the sterilization time the solution is cooled down to a temperature within the metastable zone and left to stabilize. Once this occurs, the pipet is put in contact to the solution and a few drops of solution brought up into the pipet, where the solution cools slowly to a temperature slightly below the edge of the metastable zone. The solution inside the pipet cavity reaches the limit of the metastable zone within a couple of minutes and nucleates; the nucleation rate under these conditions is not only low but also slows down rapidly according to eq 11 because the driving force for crystallization diminishes with every new nucleus that appears. The nuclei grow and deplete the supersaturation in the pipet. After a few minutes the nucleated solution, which usually contains only a few micro crystals, is returned to the mother solution. The temperature of the mother solution is kept constant during the whole procedure. The effect of the cooled unsaturated drops of solution as they enter the mother solution should be negligible and the micro crystals are then inside a slightly supersaturated solution, which allows them to grow relatively slow and in a constant manner as compared to the conditions that prevail when spontaneous nucleation occurs. It is usually not necessary to lower the temperature of the mother solution after the nucleation because the mass of crystal grown is small enough not to deplete the driving force for crystallization in the short time required to obtain small platelets.[33]

The crystals obtained in this manner have areas that normally range from 1 × 1 mm^2 to 5 × 5^2 for the ***ab*** face and thicknesses that range from 0.2 mm to 1.5 mm in the ***c*** direction. The size of the crystals depends on the parameters chosen for the experiment described above. The growth time of the plates varies from 1 to 3 days. Figure 9 shows a schematic temperature profile inside of the pipet for such a system. Here we consider that 0.05 mL of the solution with concentration that corresponds to an equilibrium temperature of T_e = 40 °C are pulled inside the pipet. The number of expected seeds at the end of the nucleation period is about 20 and the sizes of the obtained nucleuses range from 50 to 150 μm in the largest side dimension.

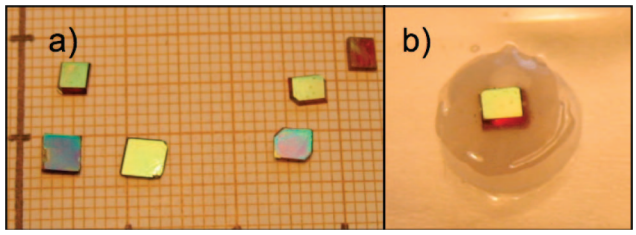

Figure 10. Plates grown by the confined spontaneous nucleation (CSN) method under various conditions: (a) DAST plates as grown, color of plates varies because of the angle at which they reflect light; (b) single crystalline plate of DAST polished on both sides and mounted for transmission experiments on quartz optical plate. Final thickness of the plate is 835 μm.

4.2.b. Processing of the Crystals Grown by CSN for THz Experiments. The plates obtained with these experiments had *ab*-face areas of a few square millimeters and a thickness of 100 μm to 1 mm in the *c* direction. The plates were of good optical quality and were polished on both sides and mounted for transmission experiments.

Figure 10 shows a photograph of a few examples of the plates obtained with this method. Although as grown DAST crystals are relatively flat and present surfaces that to the eye look almost as polished, there is still the need to polish them on both sides for nonlinear optics experiments due to the nature of the growth of DAST crystals. The mechanism of growth is a two-dimensional nucleation of a new layer or step on the a corner of the crystal that then spreads over the *ab* face toward the *-a* direction; this same mechanism repeats itself on (001) and (00$\bar{1}$) with a higher rate of nucleation of new steps on the (001) face as the one of (00$\bar{1}$). The result is a slightly higher thickness (*c*-dimension) of the crystal on the area closest to the *a* corner as that of the one closest to the *-a* corner (Figure 7). The thickness varies in steps that can be easily seen under microscope. The terraces usually have sudden drops of up to 1 μm, while the area of each terrace is variable and depends on the two-dimensional nucleation rate in relationship to their superficial extension. As a rule of thumb, the two-dimensional nucleation rate is higher for crystals grown at higher temperatures/concentrations. Although this effect might be negligible in some cases or irrelevant for reflection applications, for NLO applications, the angle between the entry and exit faces of the crystal can be enough to distort the wave propagation. In Figure 10a, we show a series of crystals grown under different conditions to obtain various thicknesses and sizes. The crystals are red in transmission and greenish in reflection, but they show different shades on reflection due to the different angle to the camera lens and the incident light. The (b) section shows a crystal that has been polished to $\lambda/4$ (λ = 632 nm) on both sides and mounted on a quartz plate of optical quality. The thickness of the crystal is 835 μm.

We have not observed any damage in the plates used for NLO experiments that have been in use for more than 5 years and also any decay in their performance; in this period, the experiment with the longest duration and maximum power was carried out with a femtosecond laser with a pulse duration of 150 fs and a maximum intensity of 30 GW/cm^2. The plates are stored at room temperature inside a desiccator when not in use, but they remain in the experiment setup for long (weeks) periods of time. Only homogeneous crystals without any visible striations, cracks or scratches are used for NLO experiments.[6,8,45,46] Photostructuring of DAST crystals for waveguide applications was successfully achieved by means of photobleaching[3,21] and femtosecond ablation[18] with lasers of wavelengths between 450 and 580 nm; in this regime the absorption of the crystals is much higher than at the telecommunication wavelengths normally used for NLO experiments. Additionally, the production of waveguides was achieved by electron beam irradiation[47] and H^+ ion implantation.[19]

4.2.c. Growth of Dimension-Tailored Crystals. The dependence of the growth speed in different crystallographic directions on the growth conditions can be used for the production of size tailored crystals for different applications. In particular we refer to the ***a/c*** ratio or side dimension to thickness ratio of the crystals. As already mentioned in Section 3.1, this slight change of the growth habit is caused by the growth mechanism of DAST crystals. The ***ab*** faces are vicinal growth surfaces and they have an angle to the singular face of the crystal, which depends on the rate of nucleation of the new step and the time it takes to the step to destroy itself by growing until the opposite edge of the crystal. For higher concentrations of the solution, the nucleation rate of additional steps is higher than at lower concentrations. Therefore, the final crystal has more ***ab*** layers and the ***a/c*** ratio is lower. Experimental measurements of the aspect ratio of crystals grown from solutions of different concentration were presented by Nagaoka et al.[43] and by using this same feature we produced a set of crystals for THz generation experiments and for the investigation of the THz bandwidth generated by optical rectification for different crystal thickness.[8,33,48] The growth of such size tailored crystals reduces the post processing time considerably as no cutting of the crystal is necessary for many applications.

4.3. Bulk Crystal Growth.

4.3.a. Measurement of the Growth Rate. The growth rate of the crystal mainly depends on the Gibbs free energy difference between the crystal and the solution from which it grows; this is the driving force for the crystal growth. The driving force in its turn depends on the supersaturation. It is common to find growth laws that depend on the supersaturation value, which can lead to confusion when the concentration and the temperature of the solution are not taken into account.

The growth rate was measured for different supersaturations for a solution with concentration 3.7 g of DAST per 100 g of methanol, which corresponds to an equilibrium temperature T_{eq} = 42 °C. The volume of the solution was 800 mL, the relatively large amount of solution was chosen so that no considerable depletion of the solution due to the growth of the seed took place. Note that depletion of the solution was still taken into account; by having a large volume the accuracy was not so much affected by the errors in the measurements of the size of the grown crystal. A single seed mounted on a holder was placed inside the overheated solution and the temperature then lowered to the equilibrium temperature. The seed was left to regenerate for approximately 10 h at this temperature. Then the temperature was lowered at a constant rate of 0.0025 °C/h using a temperature controller which has an accuracy of 0.001 °C. A photograph of the crystal was taken every 24 h and the dimensions of the ***ab*** face were measured to determine the lateral growth of the crystal. The growth rate on the ***c*** direction was not measured, but it is usually about 5 times lower than the one for the lateral growth, which was considered for the evaluation of the volume of the grown crystal.

The crystal size was measured for a total of 41 days. The maximum supersaturation measured was S = 1.13, which corresponds to a temperature T = 39.6 °C for the concentration used, which was depleted by only about 1% to this point, and an excess Gibbs free energy density ΔG_{Vsol} of 22.7 mJ/mL.

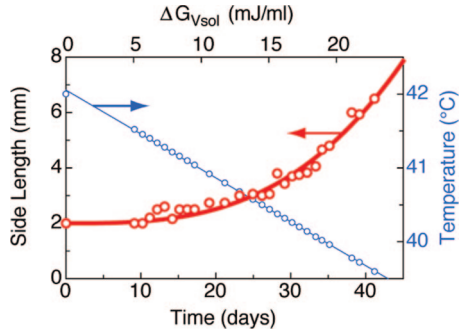

Figure 11. Crystal side length as a function of the growth time and ΔG_{Vsol} for the linear cooling rate with the corresponding temperature shown on the right scale. The thick solid line corresponds to the theoretical growth rate according to eq 20, which is also shown in Figure 12. The DAST/methanol solution had an initial concentration of 3.7 g/100 mL which corresponds to an equilibrium temperature $T_{eq} = 42$ °C.

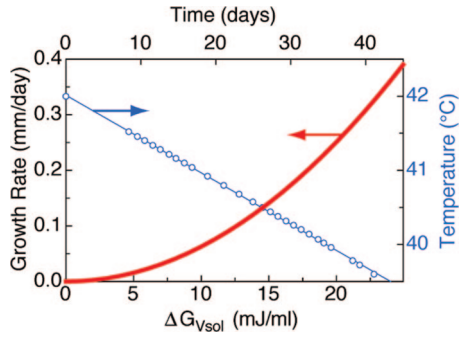

Figure 12. Growth rate according to eq 20 for the experiment of Figure 11 as a function of ΔG_{Vsol} and the growth time. The cooling rate was linear; the corresponding temperature is shown on the right scale.

Figure 11 shows the development of the crystal size as a function of time during the measured period.

It was not possible to measure a reliable growth rate beyond the above-mentioned supersaturation because the induction time was reached. Secondary nucleation happened after 32 days of continuous cooling. Nevertheless, the nucleation rate was very low with approximately 120 seeds observed in the system.

Figure 12 shows the corresponding growth rate as a function of the excess Gibbs free energy density ΔG_{Vsol}. As discussed in Sections 2.4 and 2.5, we find this measure more useful than the more commonly used supersaturation, because the growth rate also has a strong dependence on the temperature and on the real concentration of the solutions. Growth rates expressed as a function of supersaturation are only valid for a certain equilibrium concentration and in narrow temperature regimes. In experiments of growth from solution by slow cooling, the real concentration varies through a large range making the supersaturation data useless. Moreover, supersaturation can be a misleading measure due to its definition. The same amount of supercooling produces a smaller amount of supersaturation at higher concentrations than at lower ones and the same amount of supersaturation produces much higher growth rates at high concentrations than at low ones.

4.3.b. Growth of DAST Crystals Using a Linear Cooling Rate. A lot of experiments have been done for the growth of crystals by numerous authors and it is common to find linear cooling rates as the main parameter of the growth. In most cases there is no mention of the amount of solution nor the initial size of the seeds used. The levels of supersaturation obtained for such cooling rates vary strongly depending on the amount of solution used and the cooling rate, and as a consequence the growth rate.

To illustrate this, we have evaluated the effect of linear cooling rates in a variety of cases (Figure 13). We considered a solution with an equilibrium temperature of 42 °C for all cases. For the first example, we chose a cooling rate of 1 °C/day until the spontaneous nucleation was reached and changed to a cooling rate of 0.1 °C/day afterward, similar to that reported by Mori et al.[13] The calculation was done considering 300 mL of solution in the system. Figure 13a, left shows the limits (red and blue lines) of the metastable zone throughout the experiment and the actual temperature (green line); on the right side of Figure 13a, the growth rate as a function of time. In the beginning of the process, the temperature is within the metastable zone edges, and there is no crystal growing inside of the solution. The zone-edge temperatures only start to decrease as the first nuclei appear and grow; after this point the supersaturation decays rapidly and so does the growth rate. The quality of the crystal can be deeply affected by these changing growth conditions. Moreover, the results of this experiment depend strongly on the amount of solution used, the amount of seeds that appear and the initial concentration of the solution; in any case the conditions are far from ideal for the production of high quality crystals.

For the case when a seed is placed inside the solution from the beginning, the growth rate first increases quadratically with time, reaches a maximum, and then decreases to stabilize in a marginal growth rate. The left side of Figure 13b shows a linear cooling rate (green line) with a single seed, which is introduced at the beginning of the experiment together with the limits of the metastable zone (red and blue lines) during the experiment as a function of time; the corresponding growth rate is shown on the right side. This simulation corresponds to 100 mL of solution and a seed of initial size $2 \times 2 \times 1$ mm^3 with a cooling rate of 1 °C/day. As a comparison, we have made the same simulation with identical conditions except for the amount of solution used, in this case 230 mL were used instead of 100 mL. Figure 13c shows the limits of the metastable zone, cooling rate, and the corresponding growth rate. There is a dramatic change in the growth rate due to the nucleation of new seeds after the eighth day.

Smaller linear cooling rates will in general result in much lower growth rates but will not improve the overall performance because the supersaturation is a function of the size of the system, the size of the seed, and the time the seed has to grow. Although by some coincidence of circumstances it may look like a certain cooling rate gives good results, in reality the cooling rate alone provides no information without considering the other variables, and evaluating the results obtained by only comparing the cooling rates is impossible.

4.3.c. Growth with Optimized Cooling Rates. Starting from the growth rates measured for a given supersaturation and concentration we can calculate the projected growth and the development of the equilibrium temperature as a function of time with the help of the mass balance equations presented in the theoretical section. For our calculations we have considered the shape of the seed to be a square plate that grows into the diagonal ***a*** direction. The seed is considered to be mounted vertically with the ***a***-axis pointing upward. The ***a/c*** ratio (lateral size to thickness) was taken to be 5 based on empirical numbers obtained from previous growth experiments.

Figure 14 shows the calculations made for a growth cell containing 755 mL of solution with a concentration 3.74 g/100

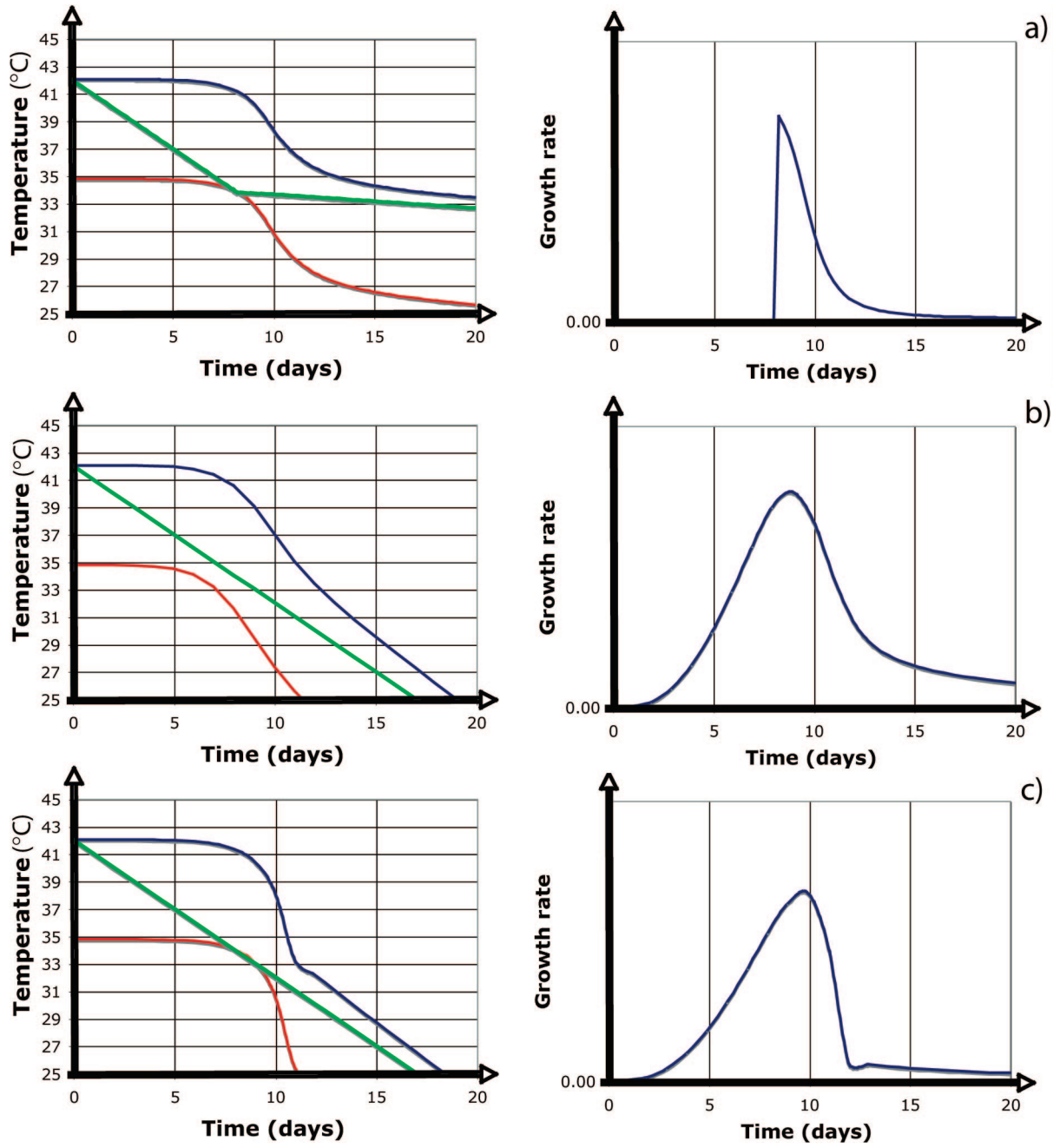

Figure 13. Metastable zone limits (left, blue and red curves) with corresponding growth rates (right) for solutions with an equilibrium temperature $T_{eq} = 42$ °C, calculated for different cooling rates (left, green curves); (a) for 300 mL of unseeded solution and a linear cooling rate of 1 °C/day until nucleation is reached and 0.1 °C/day thereafter; (b) for 100 mL of seeded solution (single 2 × 2 × 1 mm^3 seed) with a linear cooling rate of 1 °C/day; (c) same as (b) but with 230 mL of solution.

g of DAST in methanol, which corresponds to a equilibrium temperature $T_{eq} = 42.23$ °C. The lateral growth rate measured for this concentration at a supersaturation $S = 1.12$ ($\Delta G_{Vsol} =$ 23.8 mJ/ml) was approximately 0.4 mm/day. The cell was not stirred during growth.

The cooling rate was programmed using a controller with an accuracy of 0.002 °C.

A photograph of the crystal was taken every day to measure the growth. The plot of the lateral size is presented in Figure 15 as a function of time. Sufficient care was taken to record the time of the photograph and plot accordingly to avoid incorrect estimation of the growth rate.

Figure 16 shows different stages of the growth of the crystal. The photographs were taken on the 1st, 8th, and 37th day of growth.

The size of the crystal when removed from the cell after 75 days was 28 × 28 × 8 mm^3. Figure 17 shows a photograph of the crystal grown while still mounted on its holder. In the mirror-like surface of the crystal it is possible to see the reflection of the millimetric paper.

The growth time of 75 days is particularly long because of the large amount of solution used for the growth. As a general rule, such long periods of growth should be avoided though, because the total growth time should not exceed the induction time of the solution for the chosen supersaturation. It is not

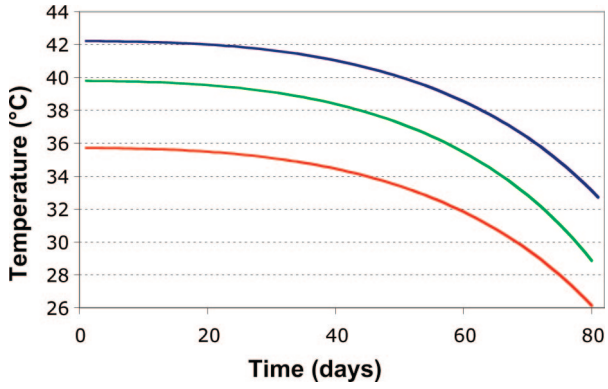

Figure 14. Optimal cooling rate for a growth cell containing 755 mL of solution with an equilibrium temperature $T_{eq} = 42.23$ °C. The initial size of the seed was $2 \times 2 \times 0.5$ mm^3. The blue line represents the equilibrium temperature, the red line is the lower edge of the metastable zone, and the green line is the necessary temperature to achieve constant growth rate.

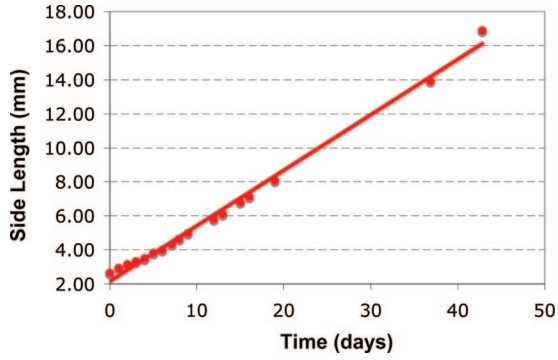

Figure 15. Measured size for the growth along the ***ab*** direction of the crystal (lateral size) as a function of time. The crystal was grown with an optimized cooling function to achieve a constant growth rate.

convenient to interrupt growth processes at high temperatures and remove the growing crystals from the growing cells; therefore, we design our experiments in such ways that the total growth time is lower than the induction time for given supersaturation and concentration and the final temperature is close to room temperature, thus avoiding thermal shocks when removing the crystals from the growth cells. We achieve this by either reducing the amount of solution in the cell or by using multiple seeds for a single run in a large cell.

An experiment with a shorter growth time was carried out with a cell containing one large seed of $3 \times 4 \times 1.5$ mm^3 and 20 smaller seeds of approximately $1 \times 1 \times 0.2$ mm^2 each.

The amount of solution used was again 755 mL. The equilibrium concentration of the solution was 3.7 g/100 g of DAST in methanol which corresponds to $T_{eq} = 42$ °C. The starting growth temperature was chosen to be 39.880 °C, and the initial supersaturation for this concentration is then $S = 1.11$. The expected growth rate for these conditions is around 0.35 mm/day. Nevertheless, the calculations were done considering a much higher growth rate of 0.5 mm/day. As a consequence we expected additional nucleation or an increased growth rate.

The growth was completed within 30 days. The observed growth rate at the end of the run was on average 0.22 mm/day. Additional nuclei appeared in the bottom of the cell as expected to compensate for the steeper supersaturation increase. Figure 19 shows a picture of the resulting crystal after being removed from its cell. The final size of the crystal was $9.4 \times 9.3 \times 2.5$ mm^3.

The experiments have been repeated in multiple growth cells with different conditions to confirm the linearity of the growth rates. The one-dimensional size of the crystals tends to increase linearly for the most part of the growth with a slight decrease toward the end of the growth run. In most cases we can attribute this to secondary nucleation, which additionally depletes the solution. We also expected a slight decrease in the diffusion of solute molecules as the viscosity of the solution increases with lower temperature.

5. Conclusions

Organic nonlinear optical single crystals have been widely recognized as having many advantages over their inorganic counterparts, but their use has been limited by the availability of large, high optical quality crystals. The growth from solution is usually avoided due to its complexity and low yield when

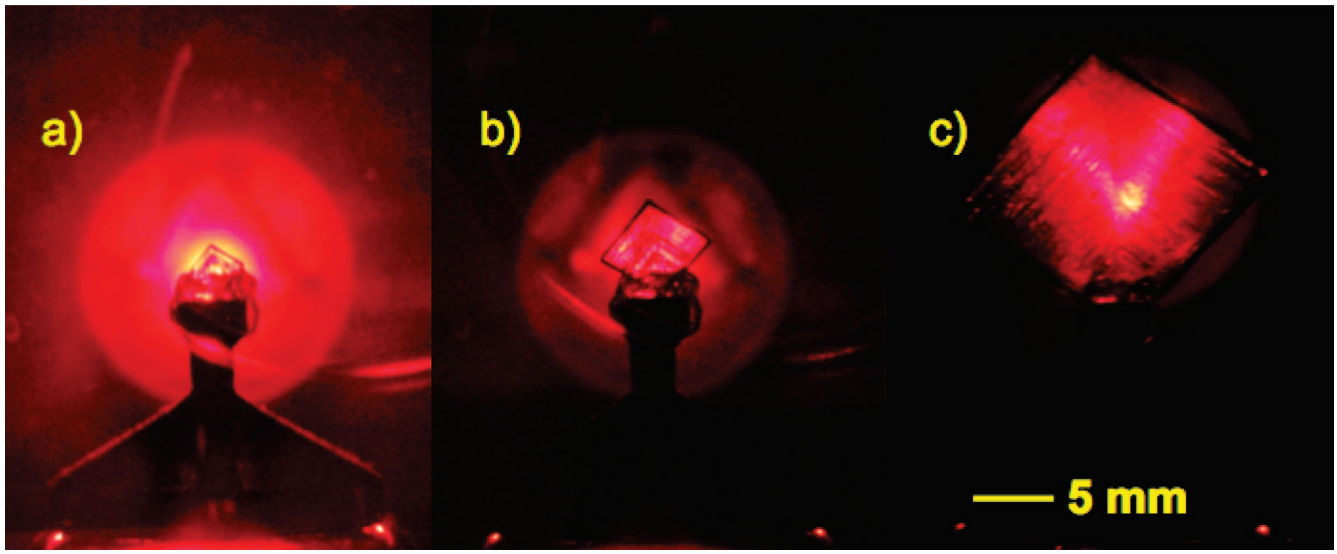

Figure 16. Growing stages of a DAST crystal with a concentration corresponding to an equilibrium temperature $T_{eq} = 42.23$ °C and an initial supersaturation of $S = 1.12$ grown under a constant free energy per unit volume of solution cooling rate ($\Delta G_{Vsol} = 23.8$ mJ/mL). The photographs correspond respectively to the (a) 1st day, (b) 8th day, and (c) 37th day of growth.

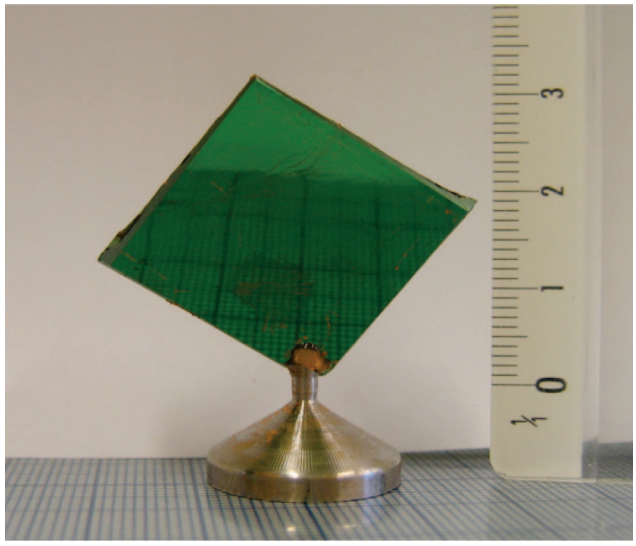

Figure 17. DAST crystal ($28 \times 28 \times 8$ mm^3) grown under the constant energy density program optimized for a growth rate of 0.4 mm/day.

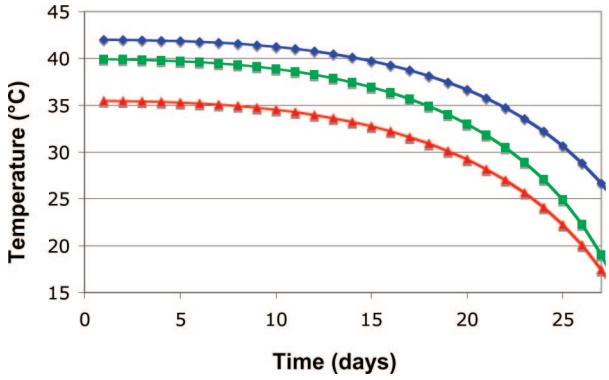

Figure 18. Optimal cooling rate for a growth cell containing 755 mL of solution with an equilibrium temperature $T_{eq} = 42$ °C and 21 seeds: one seed was $3 \times 4 \times 1.5$ mm^3 and the other 20 were $1 \times 1 \times 0.2$ mm^2. The blue line represents the equilibrium temperature, the red line is the lower edge of the metastable zone, and the green line is the necessary temperature to achieve a constant growth rate.

compared to growth from the melt; however, with a deeper understanding of the thermodynamic processes behind the growth of crystals it is possible to improve the yield and quality manifold. We have presented a complete characterization of the DAST/methanol system and determined the change of entropy and enthalpy upon dissolution for further analysis of the growth parameters.

The average surface energy was determined using the nucleation theory and experimental measurements of the induction time, which let us estimate the size of the critical nucleus.

We have described the mechanisms of growth for DAST crystals as well as the most significant morphology features affecting the growth.

The analysis of the nucleation behavior of DAST crystals has led us to develop the CSN technique for the controlled nucleation of seeds and the production of small platelets for nonlinear optical and electro-optical applications. By controlling the regime of growth we are able to influence the thickness to lateral size ratio of the resulting crystals, which reduced the postprocessing work greatly; the resulting crystals are completely homogeneous and have been used successfully in THz

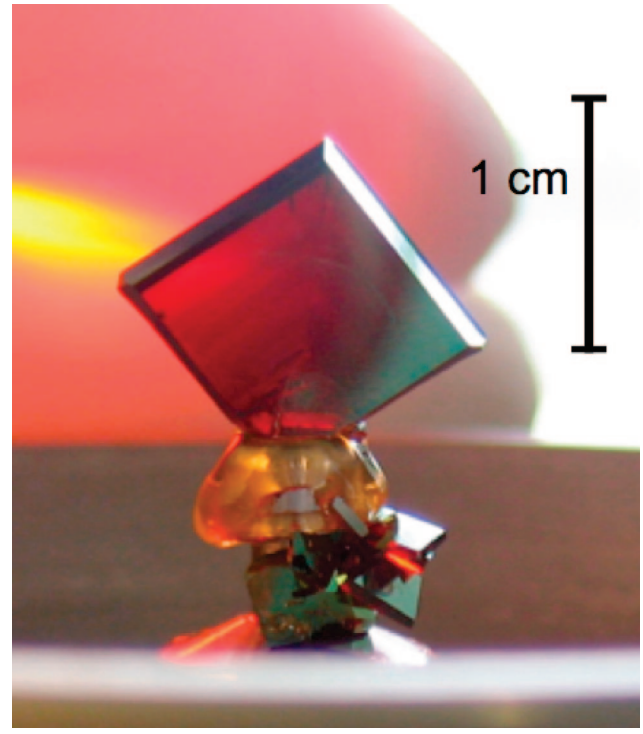

Figure 19. Crystal grown from solution with an equilibrium temperature $T_{eq} = 42$ °C and initial supersaturation of $S = 1.11$. The final size of the crystal was $9.4 \times 9.3 \times 2.5$ mm^2.

experiments for the past few years with no signs of decay in their efficiency.

We have proposed a new quantity; the excess Gibbs free energy density, that essentially affects the growth rate and includes the strong dependence on concentration of the solutions and growth temperature. The growth rate as a function of the excess free energy density is a much better measure of the development of the crystal size than the traditional growth rates as a function of supersaturation. On this basis we have developed a model to calculate the ideal temperature profile for the growth of crystals with a constant growth rate for a general system working under the slow cooling method. The constant growth rate improves the homogeneity of the resulting crystals.

By evaluating the effect of the more commonly used linear cooling rates we can show that the growth rate varies dramatically during the experiment. Using linear cooling rates, the growth rate of the crystal is almost zero during most of the growth period, and increases by more than an order of magnitude during a short time only to drop again to a marginally small growth rate, thus producing poor quality crystals in the best of cases and spontaneous nucleation in general. Also importantly, it becomes apparent that the comparison between the work done by different authors is very difficult since it strongly depends on the details of the growth system used, which is in general not documented well enough.

Using our theoretical results, we have grown record size crystals of good optical quality of up to $28 \times 28 \times 8$ mm^3 in record time.

The defects usually observed in crystals grown by not carefully regarding these considerations originate often from limitations of the profiles and equipment used rather than from fundamental limitations.

The fundamental considerations describing the growth parameters of DAST solutions in methanol should stimulate further work on improving the quality, size and growth times. This will

simplify the use of organic NLO crystals for applications in nonlinear optics such as the efficient generation of THz waves or ultrafast electro-optical switching and modulation.

Acknowledgment. The authors thank Reto Gianotti for the synthesis of materials, Marcel Sturzenegger for technical support, Jaroslav Hajfler for crystal polishing and processing, and Rainbow Photonics for the use of their laboratory facilities. This work was supported by the Swiss National Science Foundation.

References

(1) Pan, F.; Knopfle, G.; Bosshard, C.; Follonier, S.; Spreiter, R.; Wong, M. S.; Gunter, P. *Appl. Phys. Lett.* **1996**, *69* (1), 13–15.
(2) Pan, F.; McCallion, K.; Chiappetta, M. *Appl. Phys. Lett.* **1999**, *74* (4), 492–494.
(3) Kaino, T.; Cai, B.; Takayama, K. *Adv. Funct. Mater.* **2002**, *12* (9), 599–603.
(4) Thakur, M.; Xu, J. J.; Bhowmik, A.; Zhou, L. G. *Appl. Phys. Lett.* **1999**, *74* (5), 635–637.
(5) Geis, W.; Sinta, R.; Mowers, W.; Deneault, S. J.; Marchant, M. F.; Krohn, K. E.; Spector, S. J.; Calawa, D. R.; Lyszczarz, T. M. *Appl. Phys. Lett.* **2004**, *84* (19), 3729–3731.
(6) Meier, U.; Bosche, M.; Bosshard, C.; Pan, F.; Gunter, P. *J. Appl. Phys.* **1998**, *83* (7), 3486–3489.
(7) Taniuchi, T.; Ikeda, S.; Okada, S.; Nakanishi, H. *Jpn. J. Appl. Phys. Part 2-Lett. Expr. Lett.* **2005**, *44* (20−23), L652−L654.
(8) Schneider, A.; Neis, M.; Stillhart, M.; Ruiz, B.; Khan, R. U. A.; Gunter, P. *Journal of the Optical Society of America B-Optical Physics* **2006**, *23* (9), 1822–1835.
(9) Marder, S. R.; Perry, J. W.; Schaefer, W. P. *Science* **1989**, *245* (4918), 626–628.
(10) Bosshard, C., Bösch, M., Liakatas, I., Jäger, M., Günter, P. *Springer Series in Optical Science*; Springer: Berlin, Heidelberg, NY, 2000; Vol. 72, pp 163−299.
(11) Pan, F.; Wong, M. S.; Bosshard, C.; Gunter, P. *Adv. Mater.* **1996**, *8* (7), 592.
(12) Adachi, H.; Takahashi, Y.; Yabuzaki, J.; Mori, Y.; Sasaki, T. *J. Cryst. Growth* **1999**, *198−199*, 568–571.
(13) Mori, Y.; Takahashi, Y.; Iwai, T.; Yoshimura, M.; Yap, Y. K.; Sasaki, T. *Jpn. J. Appl. Phys.* **2000**, *39* (10A), L1006−L1008.
(14) Tsunesada, F.; Iwai, T.; Watanabe, T.; Adachi, H.; Yoshimura, M.; Mori, Y.; Sasaki, T. *J. Cryst. Growth* **2002**, *237*, 2104–2106.
(15) Kumar, R. M.; Babu, D. R.; Ravi, G.; Jayavel, R. *J. Cryst. Growth* **2003**, *250* (1−2), 113–117.
(16) Hameed, A. S. H.; Yu, W. C.; Tai, C. Y.; Lan, C. W. *J. Cryst. Growth* **2006**, *292* (2), 510–514.
(17) Manetta, S.; Ehrensperger, M.; Bosshard, C.; Gunter, P. *C. R. Phys.* **2002**, *3* (4), 449–462.
(18) Dittrich, P.; Bartlome, R.; Montemezzani, G.; Gunter, P. *Appl. Surf. Sci.* **2003**, *220* (1−4), 88–95.
(19) Mutter, L.; Guarino, A.; Jazbinsek, M.; Zgonik, M.; Gunter, P.; Dobeli, M. *Opt. Express* **2007**, *15* (2), 629–638.
(20) Han, P. Y.; Tani, M.; Pan, F.; Zhang, X. C. *Opt. Lett.* **2000**, *25* (9), 675–677.
(21) Mutter, L.; Jazbinsek, M.; Zgonik, M.; Meier, U.; Bosshard, C.; Gunter, P. *J. Appl. Phys.* **2003**, *94* (3), 1356–1361.
(22) Yang, Z.; Aravazhi, S.; Schneider, A.; Seiler, P.; Jazbinsek, M.; Gunter, P. *Adv. Funct. Mater.* **2005**, *15* (7), 1072–1076.
(23) Yang, Z.; Jazbinsek, M.; Ruiz, B.; Aravazhi, S.; Gramlich, V.; Gunter, P. *Chem. Mater.* **2007**, *19* (14), 3512–3518.
(24) Yang, Z.; Worle, M.; Mutter, L.; Jazbinsek, M.; Gunter, P. *Cryst. Growth Des.* **2007**, *7* (1), 83–86.
(25) Ruiz, B.; Yang, Z.; Gramlich, V.; Jazbinsek, M.; Gunter, P. *J. Mater. Chem.* **2006**, *16* (27), 2839–2842.
(26) Yang, Z.; Mutter, L.; Stillhart, M.; Ruiz, B.; Aravazhi, S.; Jazbinsek, M.; Schneider, A.; Gramlich, V.; Gunter, P. *Adv. Funct. Mater.* **2007**, *17*, 2018–2023.
(27) Ruiz, B.; Coe, B. J.; Gianotti, R.; Gramlich, V.; Jazbinsek, M.; Gunter, P. *CrystEngComm* **2007**, *9* (9), 772–776.
(28) Laveant, P.; Medrano, C.; Ruiz, B.; Gunter, P. *Chimia* **2003**, *57* (6), 349–351.
(29) *Institute of Quantum Electronics, Nonlinear Optics Laboratory Annual Report 2001*; ETH Zürich: Zürich, http://www.nlo.ethz.ch/dl/JB2001.pdf.
(30) *Institute of Quantum Electronics, Nonlinear Optics Laboratory Annual Report 2002*; ETH Zurich: Zurich, http://www.nlo.ethz.ch/dl/JB2002.pdf.
(31) *Institute of Quantum Electronics, Nonlinear Optics Laboratory Annual Report 2003*; ETH Zurich: Zurich, http://www.nlo.ethz.ch/dl/JB2003.pdf.
(32) *Institute of Quantum Electronics, Nonlinear Optics Laboratory Annual Report 2004*; ETH Zurich: Zurich, http://www.nlo.ethz.ch/dl/JB2004.pdf.
(33) Ruiz, B.; Schneider, A.; Manetta, S.; Jazbinsek, M.; Gunter, P. Growth of Thin Plates of DAST and Thin Films for Nonlinear Optic Applications, In *Conference on Lasers and Electro-Optics Europe*; Munich, Germany, June, 12−17, 2005; The Optical Society: Washington, DC, 2005; pp 308−308.
(34) Hosokawa, Y.; Adachi, H.; Yoshimura, M.; Mori, Y.; Sasaki, T.; Masuhara, H. *Cryst. Growth Des.* **2005**, *5* (3), 861–863.
(35) Brahadeeswaran, S.; Onduka, S.; Takagi, M.; Takahashi, Y.; Adachi, H.; Yoshimura, M.; Mori, Y.; Sasaki, T. *J. Cryst. Growth* **2006**, *292* (2), 441–444.
(36) Yu, W. C.; Hameed, A. S. H.; Chen, Z. B.; Tai, C. Y.; Lan, C. W. *J. Cryst. Growth* **2005**, *282* (1−2), 117–124.
(37) Hameed, A. S. H.; Rohani, S.; Yu, W. C.; Tai, C. Y.; Lan, C. W. *J. Cryst. Growth* **2006**, *297* (1), 146–151.
(38) Bardsley, W.; Hurle, D. T. J.; Mullin, J. B. *Crystal Growth: A Tutorial Approach*, 1st ed.; North-Holland Publishing Company: Amsterdam, 1977; Vol. 2, p 408.
(39) Pamplin, B. R., *Crystal Growth*, 1st ed.; Pergamon Press: Oxford, 1975; Vol. 6, p 672.
(40) Brice, J. C., *Crystal Growth Processes*, 1st ed.; Blackie and Son: London, 1986.
(41) Bennema, P. *J. Cryst. Growth* **1967**, *1*, 278–286.
(42) Sohma, S.; Takahashi, H.; Taniuchi, T.; Ito, H. *Chem. Phys.* **1999**, *245* (1−3), 359–364.
(43) Nagaoka, K.; Adachi, H.; Brahadeeswaran, S.; Higo, T.; Takagi, M.; Yoshimura, M.; Mori, Y.; Sasaki, T. *Jpn. J. Appl. Phys. Part 2* **2004**, *43* (2B), L261−L263.
(44) Takahashi, Y.; Adachi, H.; Taniuchi, T.; Takagi, M.; Hosokawa, Y.; Onzuka, S.; Brahadeeswaran, S.; Yoshimura, M.; Mori, Y.; Masuhara, H.; Sasaki, T.; Nakanishi, H. *J. Photochem, Photobiol. A* **2006**, *183* (3), 247–252.
(45) Schneider, A.; Biaggio, I.; Gunter, P. *Opt. Commun.* **2003**, *224* (4−6), 337–341.
(46) Schneider, A.; Biaggio, I.; Gunter, P. *Appl. Phys. Lett.* **2004**, *84* (13), 2229–2231.
(47) Mutter, L.; Koechlin, M.; Jazbinsek, M.; Gunter, P. *Opt. Express* **2007**, *15*, 16828–16838.
(48) Schneider, A.; Gunter, P. *Ferroelectrics* **2005**, *318*, 83–88.

CG8003432